Original Article

Institution of MECHANICAL ENGINEERS
Journal of MECHANICAL ENGINEERING SCIENCE

Proc IMechE Part C:
J Mechanical Engineering Science
0(0) 1–12

DOI: 10.1177/0954406214523581
pic.sagepub.com
SAGE

Motion analysis of a rotor supported by self-acting axial groove gas bearing system with double time delays

YF Zhang[1,2], S Zhang[3], FX Liu[3], C Zhou[3], YJ Lu[2,3,4] and N Müller[4]

Abstract

A rotor system with double time delays supported by the high-speed self-acting gas-lubricated bearings with three-axial grooves is modeled to implement active delay control of the system. The differential transformation method is employed to solve the time-dependent compressible gas Reynolds equation due to its rapid convergence rate and minimal calculation error. Based on the precise integration method, a calculation method is proposed to analyze the dynamic responses of a gas bearing-rotor nonlinear system with time delays. The motion analysis of the self-acting gas-lubricated bearing-rotor system with double time delays is implemented by the orbit diagrams, the time series, and the phase diagrams. The influence of time delays and feedback control gains on the dynamic responses of the bearing-rotor nonlinear system is analyzed. The numerical results show that the amplitude of the responses of the system with time delays control is reduced, the motion is more stable and good control effect is achieved when the chosen feedback control gains match the time delays of the bearing-rotor system.

Keywords

Self-acting gas bearing with three-axial grooves, time delay, differential transformation method, precise integration method, stability

Date received: 27 November 2013; accepted: 17 January 2014

Introduction

Gas lubrication between the rotor and the bearing has been widely applied to rotating machinery that operates at high speed and efficiency but is of lightweight.[1–5] The performances of the hydrostatic gas journal bearings and the flexure pivot hydrostatic gas tilting-pad bearings were investigated theoretically and experimentally by Liu et al.[6] and Zhu and Andres.[7] Their works provided better support in the application of the hydrostatic gas bearings for oil-free turbomachinery. Yang et al.[8,9] analyzed the dynamic coefficients and stability of the aerodynamic tilting-pad journal bearings using the linear theory. Due to the nonlinear characteristics of the gas bearings, the nonlinear theory has to be employed in nonlinear analysis of the gas bearings. Bou-Saïd et al.[10] utilized the linear and nonlinear methods to study aerodynamic foil bearings with simple flexible rotors. Their work indicated that the nonlinear method must be employed to reveal the dynamic performance of the bearings with the big eccentricities as the linear methods fail. Wang et al.[11] and Wang[12] studied the nonlinear dynamic behaviors of the cylindrical gas bearings and the herringbone-grooved gas journal bearings with a flexible rotor using the nonlinear theory. They solved the cylindrical and herringbone-grooved gas-lubricated Reynolds equations by taking the short bearing model assumption (i.e., the circumferential pressure flow of the bearing is neglected). More recently, Wang and Yau[13] and Wang[14] investigated the nonlinear behaviors of a spherical gas-lubricated bearing with a rigid and a flexible rotor, respectively, by the hybrid method of the finite difference and the differential transformation methods (DTMs). The evolution of the nonlinear responses was studied systematically by using the unbalanced

[1]School of Printing and Packaging Engineering, Xi'an University of Technology, Xi'an, China
[2]State Key Laboratory of Mechanical Transmission, Chongqing University, Chongqing, China
[3]School of Mechanical and Precision Instrument Engineering, Xi'an University of Technology, Xi'an, China
[4]College of Engineering, Michigan State University, East Lansing, MI, USA

Corresponding author:
YJ Lu, School of Mechanical and Precision Instrument Engineering, Xi'an University of Technology, Xi'an 710048, China.
Email: yanjunlu@xaut.edu.cn

mass of the rotor and the bearing number as the system parameters. Yang et al.[15] investigated the periodic solutions and their stability of the cylindrical gas journal bearing-rotor system. They obtained two threshold values of the system parameters by taking the mass of the rotor, periodic external excitation, and width-to-diameter ratio as the system parameters. Zhang et al.[16] studied the nonlinear responses of the rotor system with cylindrical gas journal bearing supports by the local iteration method and analyzed the bifurcation scenario of the responses. The preceding studies focused on the aerodynamic cylindrical gas bearing-rotor system. The load-carrying capacity of aerodynamic cylindrical gas bearings is higher but less stable. The way to overcome this shortcoming is that the axial groove is designed in the inner surface of the bearing along the axial direction. Therefore, the axial-grooved gas bearing can prevent the pressure perturbation from spreading along the axial direction. Wang et al.[17] studied the nonlinear responses and bifurcation of a two-axial grooves gas bearing-flexible rotor system by the finite difference method and Euler integration method. Rashidi Maibodi et al.[18–20] investigated the nonlinear behaviors and bifurcation of a symmetrical rigid rotor supported in non-circular gas bearings using the trajectory diagrams, the power spectra, and the Poincaré maps. In their works, the nonlinear gas film forces of two-lobe, three-lobe, and four-lobe noncircular gas-lubricated journal bearings were solved by the finite element method. The effects of pre-load and mass unbalance on nonlinear dynamic behaviors were analyzed. By using the DTM, Lu et al.[21] investigated the nonlinear behavior and bifurcation of the rigid rotor system with fixed-tilting-pad combination gas bearings support and analyzed the effects of the pre-load coefficient and the pivot ratio on the system responses.

Time delays usually deteriorate the stability of the system, cause the complex dynamic behaviors, and increase the difficulty of system control. In practice, although various measures were used to improve the actuation speed of the actuators and the sensors in the precision high/super high-speed rotor systems, the time delays phenomenon still cannot be eliminated in the active control. Because it takes time that the sensors process the signal, the actuators receive signal and exert the control force to the system in active control for the system, and the effects of inevitable time delays on nonlinear dynamic characteristics of precision high/ super high-speed gas bearing-rotor system must be considered in the studies. Alims et al.[22] proposed a method to obtain time delay values of the stable region for the feedback control systems with time delays. Meanwhile, they pointed out that the stability region of the system still exists when the double time delay values exceed the maximum allowable value for determining stability. By analyzing the transcendental characteristic equations of the responses of the magnetic bearing system, Ji[23] studied the effects of time delays on the linear stability of the system in the feedback control, and pointed out that Hopf bifurcation of the system will be exhibited when the time delay values exceed certain thresholds. More recently, Ji and Hansen[24] investigated the stability and dynamic performance of the Van der Pol-Duffing oscillator in the linear and nonlinear feedback control. When the time delays were taken as the bifurcation parameters, equilibrium point solutions exhibited the Hopf bifurcation and the inverted Hopf bifurcation with the change of time delays. By adopting the precise integration method, dynamic responses of the system with time delays were solved by Sun et al.[25] They obtained the distribution of stable regions of the system and discussed the influence of time delays and feedback control gains on distribution of stable regions of the system.

In order to reduce the calculation cost of solving the gas film forces of the self-acting gas-lubricated bearing with three-axial grooves by an iterative method and to improve the calculation accuracy, the DTM[26–29] is employed to solve pressure distribution of the nonlinear gas film. An algorithm is proposed to calculate the nonlinear dynamic behaviors of the rotor system supported on the self-acting gas-lubricated bearings with three-axial grooves based on the precise integration method[30] because the common algorithms cannot be used to calculate the nonlinear dynamic behavior of the gas bearing-rotor system with the time delay properties and the time delays control.

Equation of system

A symmetrical flexible rotor system supported on the self-acting gas bearings with three-axial grooves is shown in Figure 1. O_1 and O_3 are the geometric centers of the gas bearing, O_2 is the geometric center of the disk.

The dynamic equation of the self-acting gas bearing-symmetrical flexible rotor system can be written as

$$\mathbf{m}\ddot{\boldsymbol{x}} + \mathbf{c}\dot{\boldsymbol{x}} + \mathbf{k}\boldsymbol{x} = \boldsymbol{f} + \boldsymbol{w} + \boldsymbol{q} \tag{1}$$

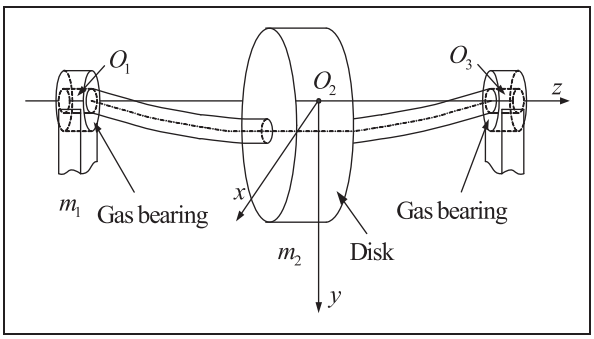

Figure 1. Schematic diagram of a symmetrical flexible rotor system supported on the self-acting gas bearings with three-axial grooves.

where $\mathbf{m}$ is the mass matrix, $\mathbf{c}$ is the damping matrix, $\mathbf{k}$ is the stiffness matrix, $\boldsymbol{x}$ is the displacement vector, $\boldsymbol{f}$ is the nonlinear gas film forces vector, $\boldsymbol{w}$ is the weight load vector, and $\boldsymbol{q}$ is the unbalanced force vector where

$$\mathbf{m} = \begin{bmatrix} m_1 & 0 & 0 & 0 \\ 0 & m_1 & 0 & 0 \\ 0 & 0 & m_2 & 0 \\ 0 & 0 & 0 & m_2 \end{bmatrix}$$

$$\mathbf{c} = \begin{bmatrix} d & 0 & -d & 0 \\ 0 & d & 0 & -d \\ -2d & 0 & 2d & 0 \\ 0 & -2d & 0 & 2d \end{bmatrix}$$

$$\mathbf{k} = \begin{bmatrix} k & 0 & -k & 0 \\ 0 & k & 0 & -k \\ -2k & 0 & 2k & 0 \\ 0 & -2k & 0 & 2k \end{bmatrix}$$

$$\boldsymbol{x} = [\,x_1 \quad y_1 \quad x_2 \quad y_2\,]^{\mathrm{T}}$$

$$\boldsymbol{f} = [\,-f_{x1} \quad -f_{y1} \quad 0 \quad 0\,]^{\mathrm{T}}$$

$$\boldsymbol{w} = [\,0 \quad m_1 g \quad 0 \quad m_2 g\,]^{\mathrm{T}}$$

$$\boldsymbol{q} = \begin{bmatrix} m_1 e_{x1}\omega^2\cos(\omega t) + m_1 e_{y1}\omega^2\sin(\omega t) \\ m_1 e_{y1}\omega^2\cos(\omega t) - m_1 e_{x1}\omega^2\sin(\omega t) \\ m_2 e_{x2}\omega^2\cos(\omega t) + m_2 e_{y2}\omega^2\sin(\omega t) \\ m_2 e_{y2}\omega^2\cos(\omega t) - m_2 \mathrm{e}_{x2}\omega^2\sin(\omega t) \end{bmatrix}$$

where x_1 and y_1 are the displacements of the journal center in the x and y directions, x_2 and y_2 are the displacements of the rotor center at disk station in the x and y directions, m_1 and m_2 are the masses lumped to the journal and the disk, respectively, $d = 24\gamma EI/l^3$ ($\gamma = 0.00193$ is the material coefficient) is the damping coefficient of the shaft, E is the elastic modulus, I is the equatorial moment of the inertial of the rotor, l is the distance between the centers of the two bearings, $k = 24EI/l^3$ is the stiffness coefficient of the shaft, f_{x1} and f_{y1} are the nonlinear gas film forces acting on the rotor in the x and y directions at left bearing station, g is the acceleration of gravity, and e_{x1}, e_{y1}, e_{x2}, and e_{y2} are the unbalanced mass eccentricities of the rotor in the x and y directions at the bearing and the disk stations. The dynamic equation of the system with time delays of speed and displacement is written in the following

$$\mathbf{m}\ddot{\boldsymbol{x}}(t) + \mathbf{c}\dot{\boldsymbol{x}}(t) + \mathbf{k}\boldsymbol{x}(t) = \boldsymbol{e}(t) + g_p\boldsymbol{x}(t - t_1) + g_d\dot{\boldsymbol{x}}(t - t_2) \tag{2}$$

where $\boldsymbol{e}(t) = \boldsymbol{f} + \boldsymbol{w} + \boldsymbol{q}$ is the excitation force vector, $g_p\boldsymbol{x}(t - t_1)$ is the control force vector corresponding to the displacement, $g_d\dot{\boldsymbol{x}}(t - t_2)$ is the control force vector corresponding to the speed, t_1 and t_2 are the values of time delays corresponding to the displacement control and the speed control, $\boldsymbol{x}(t - t_1)$ is 0 as t is less than t_1, and $\dot{\boldsymbol{x}}(t - t_2)$ is 0 as t is less than t_2.

In order to simplify calculation, the rotating speed of the rotor ω, the radial clearance of the bearing c, ambient pressure p_a, and the radius of bearing journal R are used to obtain the dimensionless dynamic equation. The dimensionless parameters are listed as follows

$$\begin{aligned} &X = \frac{x}{c}, \quad Y = \frac{y}{c}, \quad X' = \frac{\dot{x}}{\omega c}, \quad Y' = \frac{\dot{y}}{\omega c}, \\ &X'' = \frac{\ddot{x}}{\omega^2 c}, \quad Y'' = \frac{\ddot{y}}{\omega^2 c}, \quad \tau = \omega t, \quad T_1 = \omega t_1, \\ &T_2 = \omega t_2, \quad G = \frac{g}{\omega^2 c}, \quad D = \mathrm{d}\omega c/p_a R^2, \\ &K = kc/p_a R^2, \quad E_{x1} = \frac{e_{x1}}{c}, \quad E_{y1} = \frac{e_{y1}}{c}, \\ &E_{x2} = \frac{e_{x2}}{c}, \quad E_{y2} = \frac{e_{y2}}{c}, \quad F_{x1} = f_{x1}/p_a R^2, \\ &F_{y1} = f_{y1}/p_a R^2, \quad M_1 = m_1 c\omega^2/p_a R^2, \\ &M_2 = m_2 c\omega^2/p_a R^2, \\ &G_p = g_p c/p_a R^2, \quad G_d = g_d \omega c/p_a R^2 \end{aligned} \tag{3}$$

Substitution of equation (3) into equation (2) gives the dimensionless dynamic equation of the flexible rotor system with double time delays supported on the gas bearings with three grooves as follows

$$\begin{aligned} &\mathbf{M}\boldsymbol{X}''(\tau) + \mathbf{C}\boldsymbol{X}'(\tau) + \mathbf{K}\boldsymbol{X}(\tau) \\ &\quad = \boldsymbol{E}(\tau) + G_p\boldsymbol{X}(\tau - T_1) + G_d\boldsymbol{X}'(\tau - T_2) \end{aligned} \tag{4}$$

Equation (4) can be rewritten as follows

$$\begin{aligned} &\begin{bmatrix} M_1 & 0 & 0 & 0 \\ 0 & M_1 & 0 & 0 \\ 0 & 0 & M_2 & 0 \\ 0 & 0 & 0 & M_2 \end{bmatrix} \begin{bmatrix} X_1'' \\ Y_1'' \\ X_2'' \\ Y_2'' \end{bmatrix} \\ &\quad + \begin{bmatrix} D & 0 & -D & 0 \\ 0 & D & 0 & -D \\ -2D & 0 & 2D & 0 \\ 0 & -2D & 0 & 2D \end{bmatrix} \begin{bmatrix} X_1' \\ Y_1' \\ X_2' \\ Y_2' \end{bmatrix} \\ &\quad + \begin{bmatrix} K & 0 & -K & 0 \\ 0 & K & 0 & -K \\ -2K & 0 & 2K & 0 \\ 0 & -2K & 0 & 2K \end{bmatrix} \\ &\quad = \begin{bmatrix} -F_{x1} \\ -F_{y1} \\ 0 \\ 0 \end{bmatrix} + \begin{bmatrix} 0 \\ M_1 G \\ 0 \\ M_2 G \end{bmatrix} + \begin{bmatrix} M_1 E_{x1}\cos\tau + M_1 E_{y1}\sin\tau \\ M_1 E_{y1}\cos\tau - M_1 E_{x1}\sin\tau \\ M_2 E_{x2}\cos\tau + M_2 E_{y2}\sin\tau \\ M_2 E_{y2}\cos\tau - M_2 E_{x2}\sin\tau \end{bmatrix} \\ &\quad + G_p \begin{bmatrix} X_1(\tau - T_1) \\ Y_1(\tau - T_1) \\ X_2(\tau - T_1) \\ Y_2(\tau - T_1) \end{bmatrix} + G_d \begin{bmatrix} X_1'(\tau - T_2) \\ Y_1'(\tau - T_2) \\ X_2'(\tau - T_2) \\ Y_2'(\tau - T_2) \end{bmatrix} \end{aligned}$$

The solution of the nonlinear gas film forces

The DTM is for solving the differential equations based on Taylor expansion.[26] Due to its rapid convergence rate and minimal calculation error, many scholars have studied DTM and applied it to engineering.[27–29] In order to reduce the calculation cost of solving the gas film forces of the self-acting gas bearing with three-axial grooves by the iterative method and improve the calculation accuracy, the DTM is employed to solve nonlinear pressure distribution of the gas film of the bearing.

The calculation coordinate for a gas journal bearing with three-axial grooves is shown in Figure 2. O_b is the center of the bearing, O_j is the center of the journal, ξ is the groove width angle, α is the arc bushing angle of each bearing bush, β is the location angle of the pad which is calculated from negative y axis to the leading edge of the first pad, φ is the dimensionless circumferential coordinate of the bearing which starts from deviation line, ϕ is the dimensionless angle which is calculated from negative y axis to gas film location, θ is the dimensionless deviation angle, R is the radius of bearing journal, h is the thickness of gas film, f_x and f_y are the nonlinear gas film forces in the negative directions of x and y axes, respectively, ω is rotational speed, and B is the width of the bearing.

The dimensionless compressible gas Reynolds equation is written as

$$\frac{\partial}{\partial\varphi}\left(PH^3\frac{\partial P}{\partial\varphi}\right)+\frac{\partial}{\partial\lambda}\left(PH^3\frac{\partial P}{\partial\lambda}\right)=\Lambda\frac{\partial(PH)}{\partial\varphi}+2\Lambda\frac{\partial(PH)}{\partial\tau} \tag{5}$$

where λ is the dimensionless axial coordinate of the bearing, $P=p/p_a$ is the dimensionless gas film pressure, p_a is the ambient pressure, $H=1+\varepsilon\cos(\phi-\theta)$ is the dimensionless thickness of gas film, $\varepsilon=\sqrt{e_x^2+e_y^2}/c$ is the dimensionless eccentricity (eccentric ratio), e_x and e_y are the mass eccentricities in the x and y directions, respectively, c is the radial clearance of the bearing, $\Lambda=\frac{6\mu\omega}{p_a}\left(\frac{R}{c}\right)^2$ is the bearing number, μ is the gas dynamic viscosity, and $\tau=\omega t$ is the dimensionless time.

The boundary conditions of the pressure distribution of the self-acting gas bearing with three-axial grooves are

1. $P_{\tilde{i}}\big|_{\varphi=\beta+(\tilde{i}-1)(\alpha+\xi)-\theta}=P_{\tilde{i}}\big|_{\varphi=\beta+\tilde{i}\alpha+(\tilde{i}-1)\xi-\theta}=1$, $P_{\tilde{i}}\left(\varphi,\ \pm\frac{B}{2R}\right)=1(\tilde{i}=1,2,3)$, where $P_{\tilde{i}}$ is the dimensionless pressure distribution of the $\tilde{i}$th pad, and $\frac{B}{2R}$ is the width-to-diameter ratio.
2. $P_{\tilde{i}}(\varphi,\lambda)=P_{\tilde{i}}(\varphi,\ -\lambda)$, $\frac{\partial P_{\tilde{i}}}{\partial\lambda}\Big|_{\lambda=0}=0$.

By using the DTM, equation (5) can be transformed as

$$\begin{aligned}&3S\otimes\frac{\partial\bar{H}}{\partial\varphi}\otimes\frac{\partial U}{\partial\varphi}+T\otimes\frac{\partial^2U}{\partial\varphi^2}\\&\quad+3S\otimes\frac{\partial\bar{H}}{\partial\lambda}\otimes\frac{\partial U}{\partial\lambda}+T\otimes\frac{\partial^2U}{\partial\lambda^2}\\&=2\Lambda\frac{\partial\bar{H}}{\partial\varphi}\otimes\bar{P}+2\Lambda\frac{\partial\bar{P}}{\partial\varphi}\otimes\bar{H}\\&\quad+4\Lambda\frac{\partial\bar{H}}{\partial\tau}\otimes\bar{P}+4\Lambda\frac{\partial\bar{P}}{\partial\tau}\otimes\bar{H}\end{aligned} \tag{6}$$

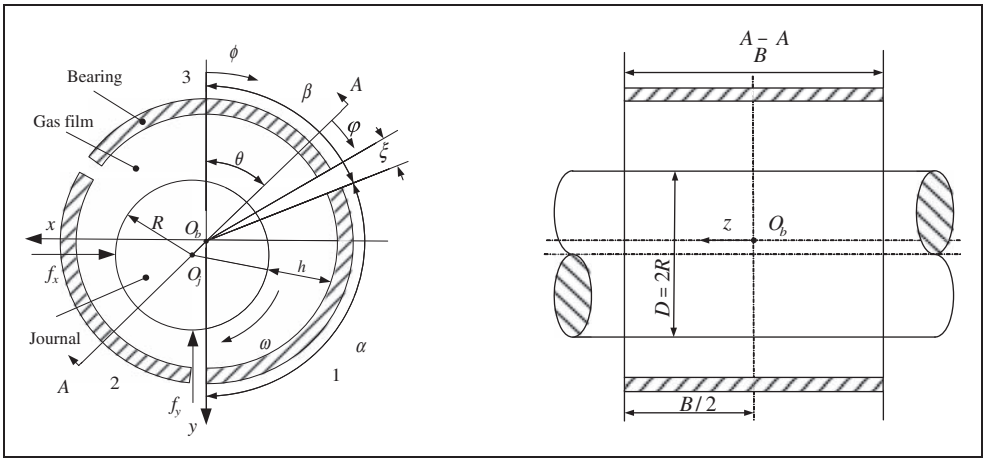

Figure 2. Calculation coordinate for the gas journal bearing with three-axial grooves.

where operator $\otimes$ represents convolution

$$U(k) = \bar{P} \otimes \bar{P} = \sum_{j=0}^{k} \bar{P}(k-j)\bar{P}(j) \tag{7}$$

where $\bar{P}$ is the image function of P

$$S(k) = \bar{H} \otimes \bar{H} = \sum_{j=0}^{k} \bar{H}(k-j)\bar{H}(j) \tag{8}$$

where $\bar{H}$ is the image function of H

$$\begin{aligned} T(k) &= \bar{H} \otimes \bar{H} \otimes \bar{H} \\ &= \sum_{j=0}^{k} \bar{H}(k-j) \sum_{i=0}^{j} \bar{H}(j-i)\bar{H}(i) \end{aligned} \tag{9}$$

By using the finite difference method to discretize equation (6) with respect to ϕ and λ, and substituting equations (7) to (9) into equation (6), the following equation (10) can be obtained

$$\begin{aligned} &3\sum_{j=0}^{k} S_{n,m}(k-j) \sum_{i=0}^{j} \left[\begin{array}{l} \left(\frac{\bar{H}_{n+1,m}(j-i)-\bar{H}_{n-1,m}(j-i)}{2\varphi}\right) \\ \times\left(\frac{U_{n+1,m}(i)-U_{n-1,m}(i)}{2\varphi}\right) \end{array} \right] \\ &\quad + \sum_{j=0}^{k} \left[\begin{array}{l} T_{n,m}(k-j)\times \\ \left(\frac{U_{n+1,m}(j)-2U_{n,m}(j)+U_{n-1,m}(j)}{(\Delta\varphi)^2}\right) \end{array} \right] \\ &\quad + 3\sum_{j=0}^{k} S_{n,m}(k-j) \sum_{i=0}^{j} \left[\begin{array}{l} \left(\frac{\bar{H}_{n,m+1}(j-i)-\bar{H}_{n,m-1}(j-i)}{2\lambda}\right) \\ \times\left(\frac{U_{n,m+1}(i)-U_{n,m-1}(i)}{2\lambda}\right) \end{array} \right] \\ &\quad + \sum_{j=0}^{k} \left[\begin{array}{l} T_{n,m}(k-j) \\ \left(\frac{U_{n,m+1}(j)-2U_{n,m}(j)+U_{n,m-1}(j)}{(\Delta\lambda)^2}\right) \end{array} \right] \\ &= 2\Lambda \sum_{j=0}^{k} \left[\left(\frac{\bar{H}_{n+1,m}(k-j) - \bar{H}_{n-1,m}(k-j)}{2\varphi} \right) \bar{P}_{n,m}(j) \right] \\ &\quad + 2\Lambda \sum_{j=0}^{k} \left[\left(\frac{\bar{P}_{n+1,m}(k-j) - \bar{P}_{n-1,m}(k-j)}{2\varphi} \right) \bar{H}_{n,m}(j) \right] \\ &\quad + 4\Lambda \sum_{j=0}^{k} \left[\left(\frac{j+1}{\tau} \right) \bar{H}_{n,m}(k-j)\bar{P}_{n,m}(j+1) \right] \\ &\quad + 4\Lambda \sum_{j=0}^{k} \left[\left(\frac{j+1}{\tau} \right) \bar{P}_{n,m}(k-j)\bar{H}_{n,m}(j+1) \right] \end{aligned} \tag{10}$$

where $\Delta\varphi$ is the circumferential step, $\Delta\lambda$ is the axial step, i, j, and k are the respective transformation orders ($k \geqslant j \geqslant i$), and n and m represent the nodal numbers of the element meshes, respectively.

The dimensionless nonlinear gas film forces of the each pad can be obtained by integrating pressure distribution in the gas field of each pad. The gas film force components of the ith pad can be expressed as follows

$$\begin{cases} F_{\tilde{i}x} = -\int_{-\frac{B}{2R}}^{\frac{B}{2R}} \int_{\beta+(\tilde{i}-1)(\alpha+\xi)-\theta}^{\beta+\tilde{i}\alpha+(\tilde{i}-1)\xi-\theta} \left[(P_{\tilde{i}}-1.0)\sin(\varphi+\theta)\right] \mathrm{d}\varphi \mathrm{d}\lambda \\ F_{\tilde{i}y} = -\int_{-\frac{B}{2R}}^{\frac{B}{2R}} \int_{\beta+(\tilde{i}-1)(\alpha+\xi)-\theta}^{\beta+\tilde{i}\alpha+(\tilde{i}-1)\xi-\theta} \left[(P_{\tilde{i}}-1.0)\cos(\varphi+\theta)\right] \mathrm{d}\varphi \mathrm{d}\lambda \end{cases} \tag{11}$$

where F_{ix} and F_{iy} are the dimensionless nonlinear gas film force components of the ith pad acting on the journal in the x and y directions.

The dimensionless nonlinear gas film force components of the self-acting gas bearing with three-axial grooves can be expressed as follows

$$\begin{cases} F_x = F_{1x} + F_{2x} + F_{3x} \\ F_y = F_{1y} + F_{2y} + F_{3y} \end{cases}$$

A method to solve equation of system based on the precise integration method

Since the precise integration method is only suitable for solving the first-order differential equation, equation (4) is expressed in the following form

$$\boldsymbol{v}'(\tau) = \mathbf{H}\boldsymbol{v}(\tau) + \boldsymbol{R}(\tau) \tag{12}$$

The following equations will be used in transformation

$$\begin{aligned} \boldsymbol{v}(\tau) &= [\boldsymbol{X}^T(\tau), \boldsymbol{p}^T(\tau)]^T \\ \boldsymbol{p}(\tau) &= \mathbf{M}\boldsymbol{X}'(\tau) + \mathbf{C}\boldsymbol{X}(\tau)/2 \\ \mathbf{H} &= \begin{bmatrix} -\mathbf{M}^{-1}\mathbf{C}/2 & \mathbf{M}^{-1} \\ \mathbf{C}\mathbf{M}^{-1}\mathbf{C}/4 - \mathbf{K} & -\mathbf{C}\mathbf{M}^{-1}/2 \end{bmatrix} \\ \boldsymbol{R}(\tau) &= [0, \boldsymbol{E}^T(\tau) + G_p\boldsymbol{X}^T(\tau - T_1) + G_d(\mathbf{M}^{-1}\boldsymbol{p}(\tau - T_2) \\ &\quad - \mathbf{M}^{-1}\mathbf{C}\boldsymbol{X}(\tau - T_2)/2)^T]^T \end{aligned} \tag{13}$$

If the system state is expressed as $\boldsymbol{v}(\tau_k)$ at the kth time step, then the system state $\boldsymbol{v}(\tau_{k+1})$ at the $(k+1)$th time step can be expressed as follows

$$\begin{aligned} \boldsymbol{v}(\tau_{k+1}) = \mathbf{T}[\boldsymbol{v}(\tau_k) + \mathbf{H}^{-1}(\boldsymbol{R}_0 + \mathbf{H}^{-1}\boldsymbol{R}_1)] \\ - \mathbf{H}^{-1}[\boldsymbol{R}_0 + \mathbf{H}^{-1}\boldsymbol{R}_1 + \boldsymbol{R}_1\delta] \end{aligned} \tag{14}$$

where δ is the time step, $\tau_k = k\delta$, $\boldsymbol{R}_0 = \boldsymbol{R}(\tau_k)$, $\mathbf{T} = \exp(\mathbf{H}\delta)$, and $\boldsymbol{R}_1 = [\boldsymbol{R}(\tau_{k+1}) - \boldsymbol{R}(\tau_k)]/\delta$.

Because the control vectors $G_pX(\tau - T_1)$ and $G_dX'(\tau - T_2)$ are related to the displacements prior to T_1 and the velocities prior to T_2, respectively, the vectors must be assigned continuously in the calculation procedure. The load vector $\boldsymbol{R}(\tau_k)$ therefore becomes the key to solve the dynamical equation of the system. The detailed calculation steps are listed as follows

Selecting the appropriate time step δ, and letting δ, T_1, and T_2 satisfy the following relations

$$\delta = T_1/l,\ \delta = T_2/p \tag{15}$$

where l and p are both positive integers. If $l < p$, the load vector of the system at the kth time step is calculated and $[\boldsymbol{X}^{\mathrm{T}}(\tau_k), \boldsymbol{p}^{\mathrm{T}}(\tau_k)]^{\mathrm{T}} = [\boldsymbol{X}_{\boldsymbol{k}}^{\mathrm{T}}, \boldsymbol{p}_{\boldsymbol{k}}^{\mathrm{T}}]^{\mathrm{T}}$ is assumed.

When $k < l - 1$ and $\delta(k+1) < \delta l = T_1$, $\boldsymbol{X}(\tau - T_1) = 0$ and $\boldsymbol{X}(\tau - T_2) = 0$ can be obtained. The load vector is expressed as follows

$$\begin{cases} \boldsymbol{R}(\tau_k) = [0, \boldsymbol{E}(\tau_k)]^{\mathrm{T}} \\ \boldsymbol{R}(\tau_{k+1}) = [0, \boldsymbol{E}(\tau_{k+1})]^{\mathrm{T}} \end{cases} \tag{16}$$

When $k = l - 1$ and $\delta(k+1) = \delta l = T_1$, $\boldsymbol{X}(\tau - T_1) = 0$ and $\boldsymbol{X}(\tau - T_2) = 0$ can be obtained. Assuming $\boldsymbol{X}(\tau_{k+1} - T_1) = \boldsymbol{X}_0$, the load vector can be expressed as follows

$$\begin{cases} \boldsymbol{R}(\tau_k) = [0, \boldsymbol{E}^T(\tau_k)]^{\mathrm{T}} \\ \boldsymbol{R}(\tau_{k+1}) = [0, \boldsymbol{E}^T(\tau_{k+1}) + G_p\boldsymbol{X}_0^{\mathrm{T}}]^{\mathrm{T}} \end{cases} \tag{17}$$

When $l \leqslant k < p - 1$ and $T_1 < \delta(k+1) < T_2$, $\boldsymbol{p}(\tau_{k+1} - T_2) = 0$ and $\boldsymbol{X}(\tau_{k+1} - T_2) = 0$ can be obtained. The load vector is expressed as follows

$$\begin{cases} \boldsymbol{R}(\tau_k) = [0, \boldsymbol{E}^T(\tau_k) + G_p\boldsymbol{X}_{\boldsymbol{k-l}}^T]^{\mathrm{T}} \\ \boldsymbol{R}(\tau_{k+1}) = [0, \boldsymbol{E}^T(\tau_{k+1}) + G_p\boldsymbol{X}_{k-l+1}^T]^{\mathrm{T}} \end{cases} \tag{18}$$

When $k = p - 1$ and $\delta(k+1) = T_2$, $\boldsymbol{p}(\tau_{k+1} - T_2) = \boldsymbol{p}_0$ and $\boldsymbol{X}(\tau_{k+1} - T_2) = \boldsymbol{X}_0$ can be obtained. The load vector is expressed as follows

$$\begin{cases} \boldsymbol{R}(\tau_k) = [0, \boldsymbol{E}^T(\tau_k) + G_p\boldsymbol{X}_{\boldsymbol{k-l}}^{\mathrm{T}}]^{\mathrm{T}} \\ \boldsymbol{R}(\tau_{k+1}) = [0, \boldsymbol{E}^T(\tau_{k+1}) + G_p\boldsymbol{X}_{k-l+1}^T \\ \quad + G_d(\mathbf{M}^{-1}\boldsymbol{p}_0 - \mathbf{M}^{-1}\boldsymbol{X}_0\mathbf{C}/2)^{\mathrm{T}}]^{\mathrm{T}} \end{cases} \tag{19}$$

When $k \geqslant p$ and $\delta(k+1) \geqslant hp = T_2$, $\boldsymbol{p}(\tau_k - T_2) = \boldsymbol{p}_0$ and $\boldsymbol{X}(\tau - T_2) = \boldsymbol{X}_0$ can be obtained. The load vector is expressed as follows

$$\begin{cases} \boldsymbol{R}(\tau_k) = [0, \boldsymbol{E}^T(\tau_k) + G_p\boldsymbol{X}_{\boldsymbol{k-l}}^T \\ \quad + G_d(\mathbf{M}^{-1}\boldsymbol{p}_{k-p} - \mathbf{M}^{-1}\boldsymbol{X}_{k-p}\mathbf{C}/2)^{\mathrm{T}}]^{\mathrm{T}} \\ \boldsymbol{R}(\tau_{k+1}) = [0, \boldsymbol{E}^T(\tau_{k+1}) + G_p\boldsymbol{X}_{k-l+1}^T \\ \quad + G_d(\mathbf{M}^{-1}\boldsymbol{p}_{k-p+1} - \mathbf{M}^{-1}\boldsymbol{X}_{k-p+1}\mathbf{C}/2)^{\mathrm{T}}]^{\mathrm{T}} \end{cases} \tag{20}$$

where the vectors such as $\boldsymbol{X}_{k\text{-}l}$, $\boldsymbol{X}_{k\text{-}p}$, and $\boldsymbol{p}_{k\text{-}p}$ are known at the kth step in calculation procedure. So, $\boldsymbol{R}(\tau_k)$ can be assigned continuously and the responses of the system can be obtained for each step. Similarly, when $l \geqslant p$, the calculation of the load vectors is similar to the preceding procedure. After the state vector of the system at the $(k+1)$th time step is calculated, the vectors of the system such as displacement and velocity can be obtained.

In order to improve the accuracy and describe the state of the system such as displacement and velocity accurately at a given time, $\boldsymbol{R}_1$ is modified by $\boldsymbol{R}_1 = [\boldsymbol{R}(\tau_{k+1}) - \boldsymbol{R}(\tau_k)]/\delta$, after $\boldsymbol{v}(\tau_{k+1})$ is calculated.

The modified $\boldsymbol{v}(\tau_{k+1})$ is substituted back to $\boldsymbol{v}(\tau_{k+1})$, iteration has to be implemented until $\max|\boldsymbol{v}^j(\tau_{k+1}) - \boldsymbol{v}^{j-1}(\tau_{k+1})| \leqslant \varepsilon$ is met (usually $\varepsilon = 10^{-8}$, j represents iteration number), and the $\boldsymbol{v}^j(\tau_{k+1})$ of iterative calculation is assigned to the initial calculated $\boldsymbol{v}(\tau_{k+1})$, i.e., $\boldsymbol{v}^j(\tau_{k+1}) \Rightarrow \boldsymbol{v}(\tau_{k+1})$.

Numerical examples and results

The parameters of the rotor and the gas bearing with three-axial grooves are listed as follows: the diameter of the shaft is 0.02 m, the length of the shaft is 0.12 m, the mass eccentricities e_x=e_y=1.0×10^{-5} m, the width of the bearing is 0.02 m, the width-to-diameter ratio is 1.0, the bushing arc angle of the bearing is 115°, the groove width angle of the bearing is 5°, the clearance of the bearing is 3.0×10^{-5} m, and the gas viscosity is 1.8×10^{-5} Pa·s.

When the time delays $T_1 = 3.14$ and $T_2 = 8.36$, the feedback control gains $G_p = -19.6$ and $G_d = -1.2$, Figure 3 shows the contrast diagrams of the motion orbits, the time series of X and Y, and the phase diagrams of Y of the centers of the journal and the disk with time delays and without time delays for rotational speed ω=1350 rad/s. It can be seen that the centers of the journal and the disk both behave as periodic motions with time delay control and without time delay control. The curves of the centers of the journal and the disk without time delays control envelop the curves of the centers of the journal and the disk with time delays control completely. If time delays control is exerted on the system, the vibration amplitudes in X and Y directions are both reduced

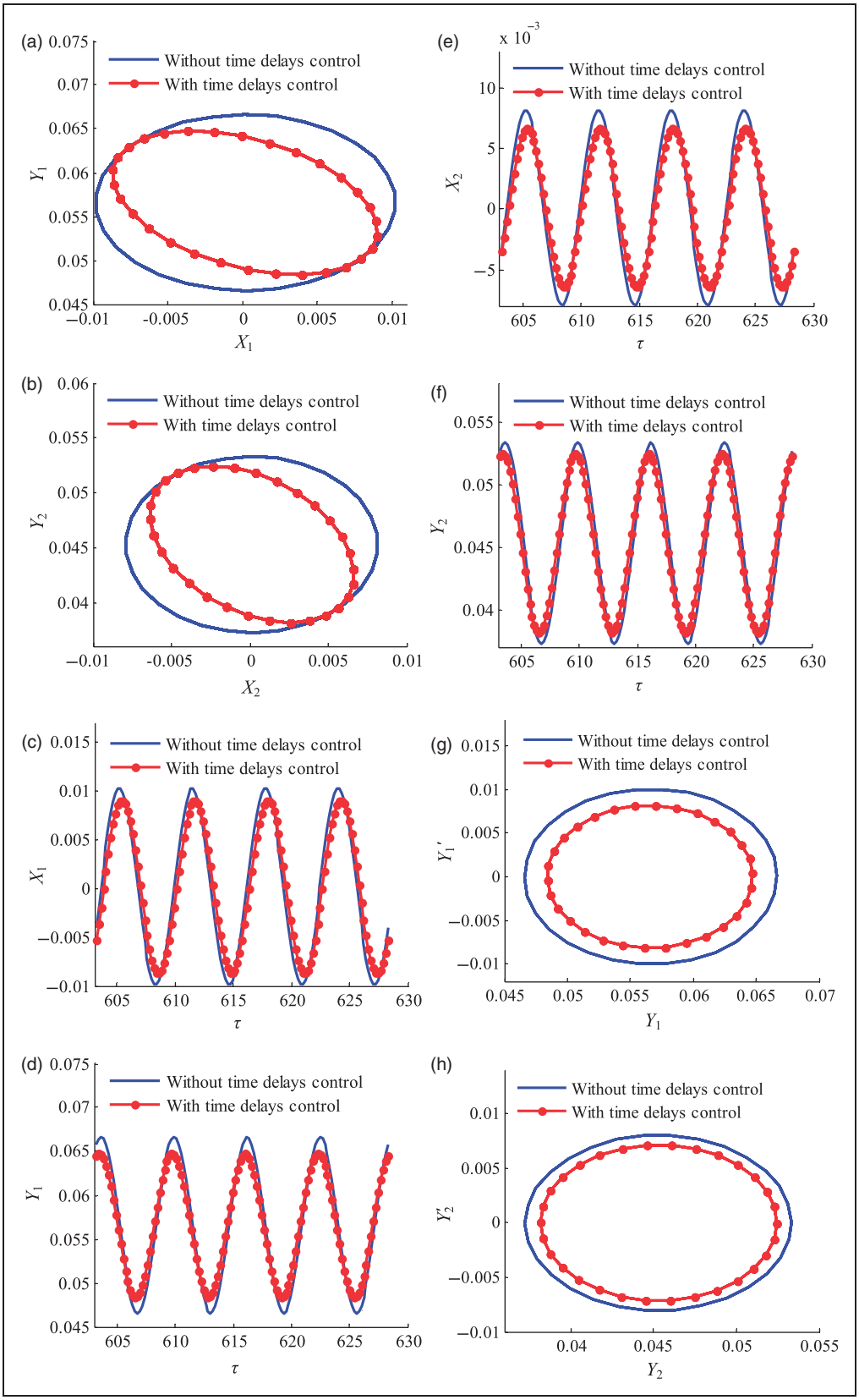

Figure 3. When the time delays $T_1 = 3.14$ and $T_2 = 8.36$, the feedback control gains $G_p = -19.6$ and $G_d = -1.2$, the contrast diagrams of the motion orbits, the time series of X and Y, and the phase diagrams of Y of the centers of the journal and the disk with time delays and without time delays for rotational speed $\omega = 1350$ rad/s. (a) The contrast diagram of the motion orbit of the journal center. (b) The contrast diagram of the motion orbit of the disk center. (c) The contrast diagram of the time series of X_1 of the journal center. (d) The contrast diagram of the time series of Y_1 of the journal center. (e) The contrast diagram of the time series of X_2 of the disk center. (f) The contrast diagram of the time series of Y_2 of the disk center. (g) The contrast diagram of the phase diagram of Y_1 of the journal center. (h) The contrast diagram of the phase diagram of Y_2 of the disk center.

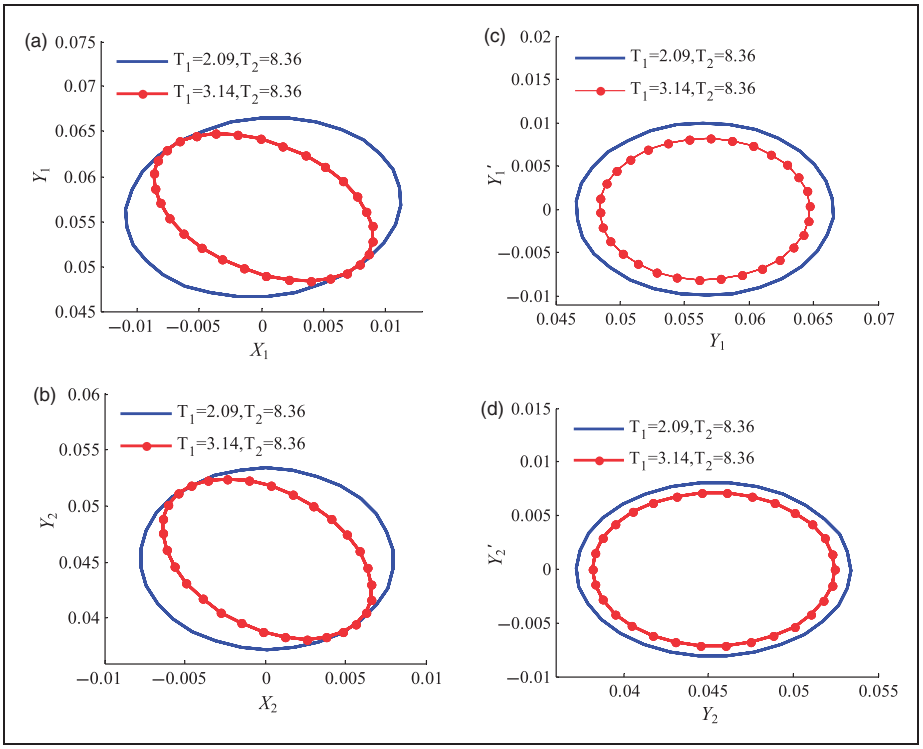

Figure 4. When time delays are: (1) $T_1 = 3.14$ and $T_2 = 8.36$, (2) $T_1 = 2.09$ and $T_2 = 8.36$, and feedback control gains are $G_p = -19.6$ and $G_d = -1.2$, the contrast diagrams of the motion orbits and the phase diagrams of Y of the centers of the journal and the disk for rotational speed $\omega = 1350$ rad/s. (a) The contrast diagram of the motion orbit of the journal center. (b) The contrast diagram of the motion orbit of the disk center. (c) The contrast diagram of the phase diagram of Y_1 of the journal center. (d) The contrast diagram of the phase diagram of Y_2 of the disk center.

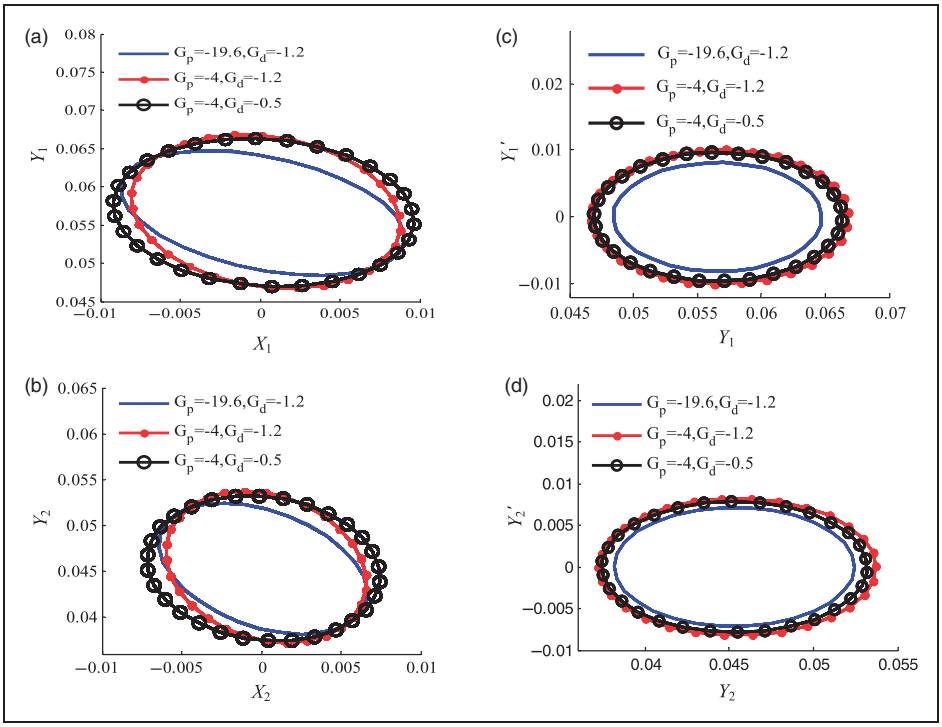

Figure 5. When feedback control gains are: (1) $G_p = -19.6$ and $G_d = -1.2$, (2) $G_p = -4$ and $G_d = -1.2$, (3) $G_p = -4$ and $G_d = -0.5$, and time delays are $T_1 = 3.14$ and $T_2 = 8.36$, the contrast diagrams of the motion orbits and the phase diagrams of Y of the centers of the journal and the disk for rotational speed ω=1350 rad/s. (a) The contrast diagram of the motion orbit of the journal center. (b) The contrast diagram of the motion orbit of the disk center. (c) The contrast diagram of the phase diagram of Y_1 of the journal center. (d) The contrast diagram of the phase diagram of Y_2 of the disk center.

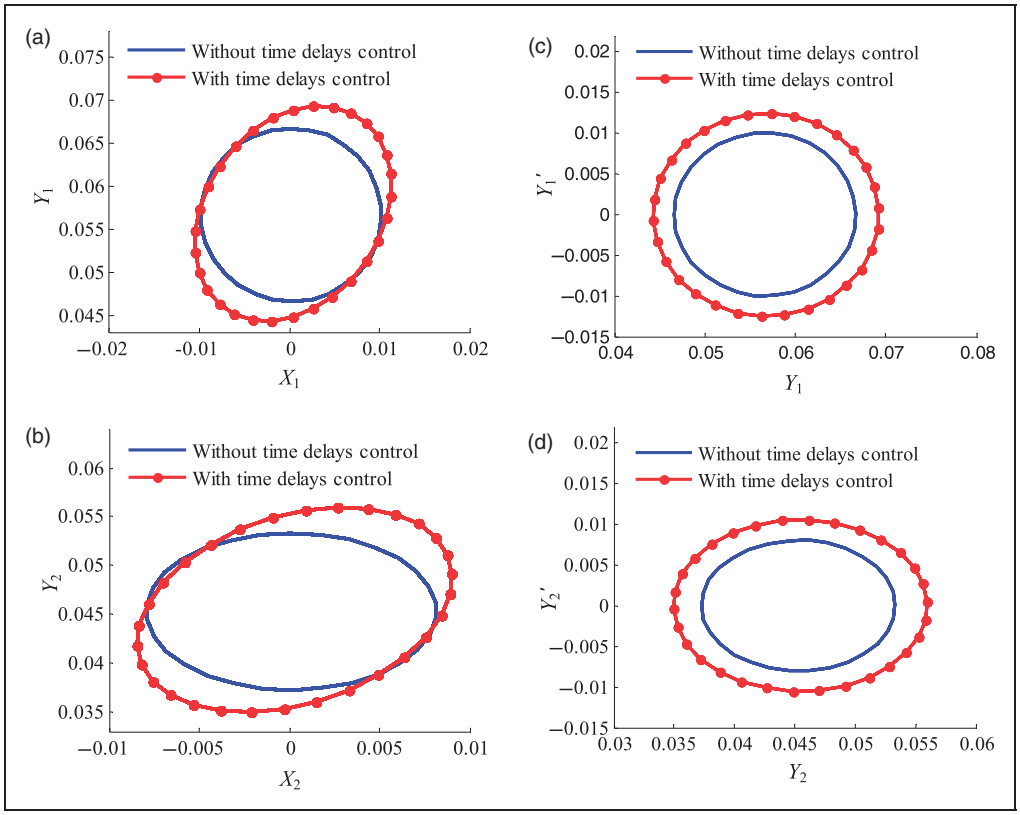

Figure 6. When the time delay $T_1 = 2.09$ and $T_2 = 3.66$, the feedback control gains $G_p = -4$ and $G_d = -1.2$, the contrast diagrams of the motion orbits and the phase diagrams of Y of the centers of the journal and the disk with time delays and without time delays for rotational speed $\omega = 1350$ rad/s. (a) The contrast diagram of the motion orbit of the journal center. (b) The contrast diagram of the motion orbit of the disk center. (c) The contrast diagram of the phase diagram of Y_1 of the journal center. (d) The contrast diagram of the phase diagram of Y_2 of the disk center.

and the vibration is located close to the axis of the centers of the journal and the disk.

When time delays are: (1) $T_1 = 3.14$ and $T_2 = 8.36$, (2) $T_1 = 2.09$ and $T_2 = 8.36$, and feedback control gains are $G_p = -19.6$ and $G_d = -1.2$, Figure 4 shows the contrast diagrams of the motion orbits and the phase diagrams of Y of the centers of the journal and the disk for rotational speed $\omega = 1350$ rad/s. It can be seen that the centers of the journal and the disk both behave as periodic motions and time delays have effects on the amplitude of the rotor. When the appropriate actuators and sensors are selected, the time delays system has appropriate time delays, the rotor system becomes more stable and the amplitude becomes smaller.

When feedback control gains are: (1) $G_p = -19.6$ and $G_d = -1.2$, (2) $G_p = -4$ and $G_d = -1.2$, (3) $G_p = -4$ and $G_d = -0.5$, and time delays are $T_1 = 3.14$ and $T_2 = 8.36$, Figure 5 shows the contrast diagrams of the motion orbits and the phase diagrams of Y of the centers of the journal and the disk for rotational speed $\omega = 1350$ rad/s. It can be seen that the amplitude of the centers of the rotor are small and more stable when the time delays are the same and the feedback control gains are $G_p = -19.6$ and $G_d = -1.2$.

When the time delay $T_1 = 2.09$ and $T_2 = 3.66$, the feedback control gain $G_p = -4$ and $G_d = -1.2$, Figure 6 shows the contrast diagrams of the motion orbits and the phase diagrams of Y of the centers of the journal and the disk with time delays and without time delays for rotational speed $\omega = 1350$ rad/s. It can be seen that the vibration amplitude of the system with time delays is increased, and the feedback control gains have important effects on the stability of the system. When the chosen feedback control gains match the time delays of the system, the amplitude of the responses of the system with time delays control is reduced and the motion is more stable. When the chosen feedback control gains do not match the time delays of the system, the amplitude of the responses of the system with time delays control is increased and the shaft may impact the inside of the bearing.

Conclusions

The dynamic equation of a flexible rotor system supported on the gas-lubricated bearings with three-axial grooves is modeled by taking the effect of the displacement time delay and the velocity time delay on the dynamic performance of the system

into consideration. The pressure distribution of the nonlinear gas film forces of the bearing with three-axial grooves is solved by the DTM. The nonlinear dynamic responses of the gas bearing-rotor system with time delays are calculated by the proposed method based on the precise integration method. The vibration amplitudes of the system with time delays and without time delays are compared and the effect of the feedback control gains on the system is analyzed.

1. To improve the calculation accuracy and reduce the calculation cost of solving the nonlinear dynamic responses of the gas bearing-rotor system, the DTM is employed to solve pressure distribution of the nonlinear gas film.
2. Based on the precise integration method, the nonlinear dynamic responses of a rotor system supported on the self-acting gas-lubricated bearings with three-axial grooves are obtained. The orbit diagrams, the time series, and the phase diagrams are employed to investigate the nonlinear unbalanced responses of the system.
3. The feedback control gains have important effects on the stability of the rotor system supported by self-acting gas-lubricated bearing with three-axial grooves. When the chosen feedback control gains match the time delays of the system, the vibration amplitude of the dynamic responses of the system becomes small, the motion is more stable and the good control effect can be achieved.

Funding

This work is supported by National Natural Science Foundation of China (Grant Nos. 51375380, 51075327), National Key Basic Research and Development Program of China (Grant No. 2013CB035705), National Natural Science Foundation of Shaanxi Province of China (Grant No. 2013JQ7008), Scientific Research Program of Shaanxi Provincial Education Department of China (Grant Nos. 12JK0661, 12JK0680), Open Project of State Key Laboratory of Mechanical Transmission (Grant No. SKLMT-KFKT-201011).

Conflict of Interest

None declared.

References

1. Rimpel A and Kim D. Rotor dynamic performance of flexure pivot tilting pad gas bearings with vibration damper. *Trans ASME J Tribol* 2009; 131: 021101–1–12.
2. Schiffmann J and Favrat D. The effect of real gas on the properties of herringbone grooved journal bearings. *Tribol Int* 2010; 43: 1602–1614.
3. Ertas BH, Camatti M and Mariotti G. Synchronous response to rotor imbalance using a damped gas bearing. *Trans ASME J Eng Gas Turbines Power* 2010; 132: 032501–1–9.
4. Zhang WM, Zhou JB and Meng G. Performance and stability analysis of gas-lubricated journal bearings in MEMS. *Tribol Int* 2011; 44: 887–897.
5. Wang CC. Bifurcation and nonlinear dynamic analysis of united gas-lubricated bearing system. *Comput Math Appl* 2012; 64: 729–738.
6. Liu LX, Teo CJ, Epstein AH, et al. Hydrostatic gas journal bearings for micro-turbomachinery. *Trans ASME J Vib Acoust* 2005; 127: 157–164.
7. Zhu XH and Andres LS. Rotor dynamic performance of flexure pivot hydrostatic gas bearings for oil-free turbomachinery. *Trans ASME J Eng Gas Turbines Power* 2007; 129: 1020–1027.
8. Yang LH, Qi SM and Yu L. Analysis on dynamic performance of hydrodynamic tilting-pad gas bearings using partial derivative method. *Trans ASME J Tribol* 2009; 131: 011703–1–8.
9. Yang LH, Qi SM, Geng HP, et al. Stability analysis on rotor systems supported by self-acting tilting-pad gas bearings with frequency effects. *Chin J Mech Eng (English edition)* 2011; 24: 380–385.
10. Bou-Saïd B, Grau G and Iordanoff I. On the nonlinear rotor dynamic effects of aerodynamic bearings with simple flexible rotors. *Trans ASME J Eng Gas Turbines Power* 2008; 130: 012503–1–9.
11. Wang CC, Jang MJ and Yeh YL. Bifurcation and nonlinear dynamic analysis of a flexible rotor supported by relative short gas journal bearings. *Chaos Solitons Fractals* 2007; 32: 566–582.
12. Wang CC. Theoretical and nonlinear behavior analysis of a flexible rotor supported by a relative short herringbone-grooved gas journal bearing system. *Physica D Nonlinear Phenom* 2008; 237: 2282–2295.
13. Wang CC and Yau HT. Application of a hybrid numerical method to the bifurcation analysis of a rigid rotor supported by a spherical gas journal bearing system. *Nonlinear Dyn* 2008; 51: 515–528.
14. Wang CC. Application of a hybrid method to the nonlinear dynamic analysis of a flexible rotor supported by a spherical gas-lubricated Bearing system. *Nonlinear Anal Theory Methods Appl* 2009; 70: 2035–2053.
15. Yang P, Zhu KQ and Wang XL. On the non-linear stability of self-acting gas journal bearings. *Tribol Int* 2009; 42: 71–76.
16. Zhang JZ, Kang W and Liu Y. Numerical method and bifurcation analysis of Jeffcott rotor system supported in gas journal bearings. *Trans ASME J Comput Nonlinear Dyn* 2009; 4: 011007–1–9.
17. Wang WM, Lü YJ, Cao ZJ, et al. Nonlinear behaviors and bifurcation of flexible rotor system with axial-grooved self-acting gas bearing support. *Adv Sci Lett* 2011; 4: 1796–1802.
18. Rashidi Maibodi R, Karami Mohammadi A and Bakhtiari-Nejad F. Bifurcation and nonlinear dynamic analysis of a rigid rotor supported by two-lobe noncircular gas-lubricated journal bearing system. *Nonlinear Dyn* 2010; 61: 783–802.
19. Rashidi Maibodi R, Karami Mohammadi A and Bakhtiari-Nejad F. Preload effect on nonlinear dynamic behavior of a rigid rotor supported by noncircular gas-lubricated journal bearing systems. *Nonlinear Dyn* 2010; 60: 231–253.
20. Rashidi Maibodi R, Karami Mohammadi A and Bakhtiari-Nejad F. Numerical analysis of a rigid rotor

supported by aerodynamic four-lobe journal bearing system with mass unbalance. *Commun Nonlinear Sci Numer Simulat* 2012; 17: 454–471.
21. Lu YJ, Zhang YF, Shi XL, et al. Nonlinear dynamic analysis of a rotor system with fixed-tilting-pad self-acting gas-lubricated bearings support. *Nonlinear Dyn* 2012; 69: 877–890.
22. Alims MS, Hou ZK and Noori MN. Stability and performance of feedback control systems with time delays. *Comput Struct* 1998; 66: 241–248.
23. Ji JC. Stability and Hopf bifurcation of a magnetic bearing system with time delays. *J Sound Vib* 2003; 259: 845–856.
24. Ji JC and Hansen CH. Stability and dynamics of a controlled van der Pol-Duffing oscillator. *Chaos Solitons Fractals* 2006; 28: 555–570.
25. Sun Q, Zhang B, Wu XH, et al. Numerical analysis for stability of trivial equilibrium solution of active control systems with double time delays (in Chinese). *J Xian Jiaotong Univ* 2010; 44: 102–106.
26. Zhao JK. *Differential transformation and its applications for electrical circuits (in Chinese)*. Wuhan: Huazhong University Press, 1986, pp.168–172.
27. Jang MJ, Chen CL and Liu YC. Two-dimensional differential transform for partial differential equations. *Appl Math Comput* 2001; 121: 261–270.
28. Abdel H and Hassan IH. Differential transformation technique for solving higher-order initial value problems. *Appl Math Comput* 2004; 154: 299–311.
29. Abdel H and Hassan IH. Comparison differential transformation technique with adomian decomposition method for linear and nonlinear initial value problems. *Chaos Solitons Fractals* 2008; 36: 53–65.
30. Zhong WX. On precise time-integration method for structural dynamics (in Chinese). *J Dalian Univ Technol* 1994; 34: 131–135.

Appendix 1

Notation

B	width of the bearing
c	radial clearance of the bearing
$\mathbf{c}$	damping matrix
d	damping coefficient of the shaft
$\mathbf{e}(t)$	excitation force vector
e_{x1}, e_{y1}	unbalanced mass eccentricities of the rotor in the x and y directions at the bearing station
e_{x2}, e_{y2}	unbalanced mass eccentricities of the rotor in the x and y directions at the disk station
E	elastic modulus
$\mathbf{f}$	nonlinear gas film force vector
f_{x1}, f_{y1}	nonlinear gas film forces acting on the rotor in the x and y directions at left bearing station
$F_{\tilde{i}x}$, $F_{\tilde{i}y}$	dimensionless nonlinear gas film forces components of the ith pad in the x and y directions ($\tilde{i}=1,2,3$)
F_x, F_y	dimensionless nonlinear gas film forces components of the self-acting gas-lubricated bearing with three-axial grooves
g	acceleration of gravity
$g_d\dot{\mathbf{x}}(t-t_2)$	control force vector corresponding to the speed
$g_p\mathbf{x}(t-t_1)$	control force vector corresponding to the displacement
G_d, G_p	feedback control gains corresponding to the speed and the displacement
H	dimensionless thickness of gas film
$\bar{H}$	image function of H
I	equatorial moment of the inertial of the rotor
k	stiffness coefficient of the shaft
$\mathbf{k}$	stiffness matrix
l	distance between the centers of the two bearings
$\mathbf{m}$	mass matrix
m_1, m_2	masses lumped to the journal and the disk respectively
O_b	center of the bearing
O_j	center of the journal
O_1, O_3	geometric centers of the gas bearing
O_2	geometric centre of the disk
p_a	ambient pressure
P	dimensionless gas film pressure
P_i	pressure distribution of the ith pad
$\bar{P}$	image function of P
$\mathbf{q}$	unbalance force vector
R	radius of bearing journal
$\mathbf{R}(\tau_k)$	load vector
$S(k)$	convolution of $\bar{H}$ and $\bar{H}$
$T(k)$	convolution of $I(n)$ and $\bar{H}$
t_1, t_2	values of time delays corresponding to the displacement control and the speed control
T_1, T_2	dimensionless values of time delays corresponding to the displacement control and the speed control
$U(k)$	convolution of $\bar{P}$ and $\bar{P}$
$\boldsymbol{v}(\tau_k)$	system state vector at the kth time step
$\boldsymbol{w}$	weight vector
$\boldsymbol{x}$	displacement vector
x_1, y_1	displacements of the journal center in the x and y directions
x_2, y_2	displacements of the rotor center at disk station in the x and y directions
α	arc bushing angle of each bearing bush
β	location angle of the pad which is calculated from negative y axis to the leading edge of the 1th pad
γ	material coefficient ($\gamma=0.00193$)
δ	time step
$\Delta\lambda$	axial step
$\Delta\varphi$	circumferential step
ε	dimensionless eccentricity ratio

θ	deviation angle
λ	dimensionless axial coordinate of the bearing
	bearing number
μ	gas dynamic viscosity
ξ	groove width angle
τ	dimensionless time
ϕ	angle which is calculated from negative y axis to gas film location
φ	dimensionless circumferential coordinate of the bearing which starts from deviation line
ω	rotating speed of the rotor
$\otimes$	convolution
$\wedge$	bearing number

Appendix 2

Dimensionless variables are as follows

D	$d\omega c/p_a R^2$
E_{xi}	$\frac{e_{xi}}{c}$
E_{yi}	$\frac{e_{yi}}{c}$
F_{x1}	$f_{x1}/p_a R^2$
F_{y1}	$f_{y1}/p_a R^2$
G	$\frac{g}{\omega^2 c}$
G_d	$g_d \omega c/p_a R^2$
H	$1+\varepsilon\cos(\phi-\theta)$
K	$kc/p_a R^2$
P	p/p_a
T_i	ωt_i $(i=1,2)$
X	$\frac{x}{c}$
X''	$\frac{c\ddot{x}}{\omega^2 c}$
Y	$\frac{y}{c}$
X''	$\frac{\ddot{y}}{\omega^2 c}$
ε	$\sqrt{e_x^2+e_y^2}/c$
τ	ωt